AGU PUBLICATIONS

JGR

Journal of Geophysical Research: Oceans

RESEARCH ARTICLE

10.1002/2015JC011565

Intensification of the subpolar front in the Sea of Japan during winter cyclones

Ning Zhao[1,2], Shinsuke Iwasaki[3], Atsuhiko Isobe[1,3], Ren-Chieh Lien[4], and Bin Wang[5]

[1]Interdisciplinary Graduate School of Engineering Sciences, Kyushu University, Kasuga, Japan, [2]Now at Research Institute for Applied Mechanics, Kyushu University, Kasuga, Japan, [3]Research Institute for Applied Mechanics, Kyushu University, Kasuga, Japan, [4]Applied Physics Laboratory, University of Washington, Seattle, Washington, USA, [5]College of Oceanography, Hohai University, Nanjing, China

Key Points:
- Extratropical cyclones generate twice stronger cooling than winter average
- SST is lowered locally along the subpolar front after cyclone passed
- Front intensification is mainly caused by the cross-frontal Ekman advection

Correspondence to:
N. Zhao,
ningz1120@riam.kyushu-u.ac.jp

Citation:
Zhao, N., S. Iwasaki, A. Isobe, R.-C. Lien, and B. Wang (2016), Intensification of the subpolar front in the Sea of Japan during winter cyclones, *J. Geophys. Res. Oceans*, *121*, doi:10.1002/2015JC011565.

Received 15 DEC 2015
Accepted 10 MAR 2016
Accepted article online 15 MAR 2016

Abstract The response of the subpolar front in the Sea of Japan (also known as the East Sea) to winter cyclones is investigated based on quantitative analyses of gridded and satellite data sets. Cyclone passages affecting the sea are detected using time series of spatially averaged surface turbulent heat fluxes. As the cyclones develop, there are strong cold-air outbreaks that produce twice the normal heat loss over the sea. After removal of sea surface temperature (SST) seasonal trends, we found that cyclone passage (hence, cooling) mainly occurred over 3 days, with maximum SST reduction of −0.4°C. The greatest reduction was found along the subpolar front, where frontal sharpness (i.e., SST gradient) increased by 0.1°C (100 km)$^{-1}$. Results of a mixed-layer model were consistent with both temperature and frontal sharpness, and localized surface cooling along the subpolar front resulted from both horizontal heat advection and turbulent heat fluxes at the sea surface. Further analyses show that this localized cooling from horizontal heat advection is caused by the cross-frontal Ekman flow (vertically averaged over the mixed layer) and strong northwesterly winds associated with the cold-air outbreak during cyclone passage.

1. Introduction

Robust relationships between oceanic fronts and the atmosphere have been demonstrated by many studies [*Small et al*., 2008, and references therein]. Atmospheric responses to the sea surface temperature (SST) field have been investigated in the context of the heat supply around oceanic fronts [e.g., *Minobe et al*., 2008], frontal strength (SST gradient) [e.g., *Nonaka et al*., 2009; *Sampe et al*., 2010], and frontal locations [e.g., *Inatsu et al*., 2003; *Ogawa et al*., 2012]. Importantly, as pointed out by *Nakamura et al*. [2004], the anchoring effect of oceanic fronts is central to modulating storm tracks and their associated polar-front jets, which may in turn drive ocean currents [*Trenberth et al*., 1990] and enhance the front itself.

Among regions with such significant air-sea coupling processes, East Asia may be one of the best known in the world. This is not only because of an oceanic front associated with a strong western boundary current, the Kuroshio, but also because there is an active region of cyclogenesis caused by both atmospheric and oceanic features [*Chen et al*., 1991, 1992; *Nakamura*, 1992; *Nakamura et al*., 2002]. Extratropical cyclones form recurrently there because of the collision between cold air from the East Asian continent and warm air masses from the ocean. These cyclones then develop above the oceanic fronts. In winter (November through February as defined in the present study), East Asia is dominated by a series of such extratropical cyclones. Of note, the Aleutian Low east of the Japanese Islands is a strong extratropical cyclone system in the winter North Pacific [*Overland et al*., 1999], provided that these cyclones develop rapidly over the East Asian continent or marginal seas and enter the North Pacific within a few days (Figure 1).

Abutting the East Asian continent, several small seas form a transition zone between the continent and North Pacific. Numerous studies have demonstrated that these marginal seas have a significant influence on regional atmospheric conditions, even extending to the North Pacific [e.g., *Hirose et al*., 2009; *Kelly et al*., 2010; *Isobe and Kako*, 2012; *Seo et al*., 2014]. Of particular interest is a two-way coupling process in the winter Yellow and East China Seas [*Iwasaki et al*., 2014]. In this process, sea surface cooling is gradually suppressed over the shallow waters because of sea level pressure (SLP; hence, winds and heat flux) modification by SST.

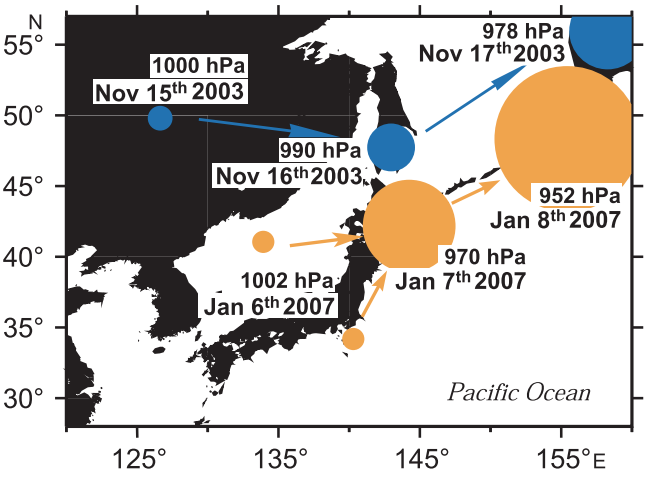

Figure 1. Study area and examples of extratropical cyclones in winter. Development of two winter cyclones based on NCEP-DOE reanalysis II data set is shown by variable circle diameter (D), according to D = 2 × (1010 − central SLP), where the SLP is regarded as a nondimensional value. Annotations near the circles denote the central SLP and date.

Among the East Asian seas, special attention should be given to the air-sea coupling processes in the winter Sea of Japan (also known as the East Sea). The reason is that this sea, at the western edge of the North Pacific, is dominated by a warm water mass where cool and dry air masses from the Asian continent first encounter. Thus, the atmosphere is strongly coupled with the ocean via intense heat and momentum fluxes. Also, there is a sharp subpolar front that separates the sea into a relatively cold and fresh subpolar region and a warm and saline subtropical region [*Isoda*, 1994; *Belkin and Cornillon*, 2003]. This front enhances low-level baroclinicity (and hence cyclone activity), as suggested by previous studies [e.g., *Yoshiike and Kawamura*, 2009; *Yamamoto and Hirose*, 2011; *Yamamoto*, 2013]. It has been shown that extratropical cyclones are enhanced above the sharper subpolar front [*Yamamoto and Hirose*, 2007]. Therefore, it is believed that the subpolar front in the Sea of Japan can be regarded as a "source region" that alters atmospheric processes over the broad East Asian region.

Although the subpolar front clearly alters extratropical cyclone activity in the Sea of Japan as described above, one may consider whether that front remains strong after extratropical cyclones. If frontal sharpness and/or location are temporarily modified by cyclone passages (as is likely because of heat fluxes through the sea surface), a two-way coupling process (i.e., air-sea interaction) may occur between the front and cyclones. In fact, it has been demonstrated that this oceanic front is strongly influenced by cooling from cyclones and their related cold-air outbreaks during winter [e.g., *Dorman et al.*, 2004; *Isobe and Beardsley*, 2007]. However, it remains unclear how the subpolar front is affected by cyclone passage, both qualitatively and quantitatively. Therefore, before considering the two-way coupling processes that may occur between the subpolar front and cyclone activity in the Sea of Japan, we quantitatively evaluate subpolar front variations during extratropical cyclone passages over the sea.

The paper is organized as follows. Section 2 presents data sources and processing. Section 3 describes analyses based on gridded data sets, followed by section 4, which introduces mechanisms of surface cooling and frontal variations over the Sea of Japan during cyclone passage, using a mixed-layer model. Section 5 gives the conclusions.

2. Materials and Methods

2.1. Data

We used four gridded data sets: SST from the National Oceanic and Atmospheric Administration Optimum Interpolation SST analysis Version 2 (OISSTv2) [*Reynolds et al.*, 2007]; SLP from the National Centers for Environmental Prediction-Department of Energy Atmospheric Model Intercomparison Project reanalysis (NCEP-DOE R2) [*Kanamitsu et al.*, 2002]; surface turbulent heat fluxes (sensible and latent heat), shortwave and longwave radiation, and 2 m air temperature from Woods Hole Oceanographic Institution (WHOI) Objectively Analyzed air-sea Fluxes (OAFlux); and ocean currents and hydrographic data from the Data assimilation Research of the East Asian Marine System (DREAMS) [*Hirose et al.*, 2013].

Wintertime 1/4° daily SST data from the period 2003 to 2011 were obtained from OISSTv2. Six-hourly mean SLP data during that period with horizontal resolution 2.5°×2.5° during the same period were acquired from NCEP-DOE R2. To align with other data sets, all SLP data were daily averaged. OAFlux offers daily 2 m air temperature and sensible and latent heat fluxes on each 1°×1° grid cell every winter from 2003 to 2011.

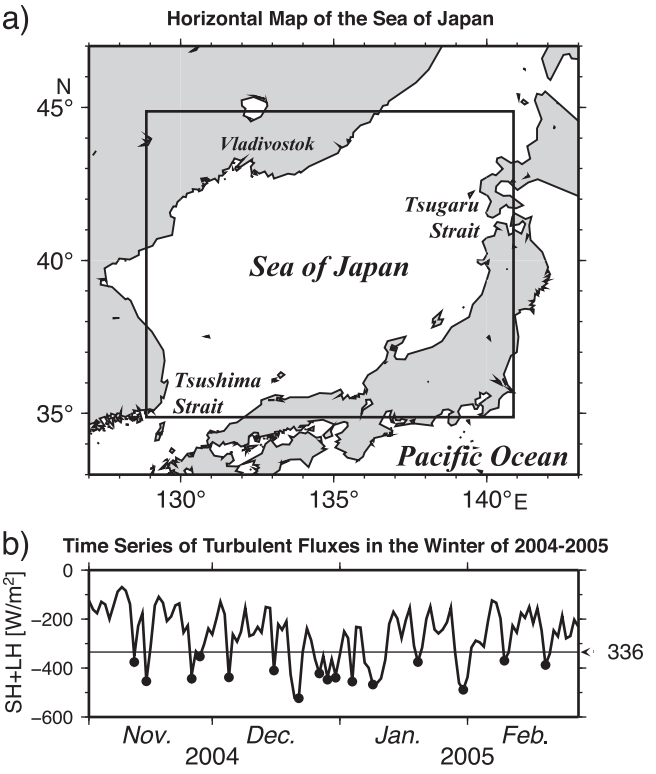

Figure 2. (a) Horizontal map of Sea of Japan, with the box over which was averaged the turbulent heat fluxes. Time series of spatially averaged turbulent fluxes in 2004–2005 winter are shown as an example in Figure 2b. Solid dots in Figure 2b show peak days (see the text for meaning), and the solid line represents the value of the eightieth percentile (-336 W/m^2).

Among the OAFlux data, the surface shortwave and longwave radiation data used by the mixed-layer model analyses (addressed later) were only available through 2009. Thus, three-dimensional oceanic data ($1/12^\circ \times 1/15^\circ$ temperature, salinity, and current velocities), which were also used by the mixed-layer model, were obtained from DREAMS for 2003–2009 only. Surface wind stress was computed using a bulk formula and satellite data from the Quick Scatterometer (QuikSCAT) and Advanced Scatterometer (ASCAT), both downloaded from the website of Remote Sensing Systems (http://www.remss.com). Wind vectors from QuikSCAT and ASCAT were simply averaged for each day during winters from 2003 to 2009, when at least one of them was available.

2.2. Data Processing

We constructed composite maps of SST and SLP based on an analysis of time series of surface turbulent fluxes. Because the passage of extratropical cyclones always results in strong turbulent heat fluxes [e.g., *Zolina and Gulev*, 2003; *Papritz et al*., 2015], we used that time series to detect cyclones affecting the Sea of Japan. Composite maps depict the modification of the SST field (and hence the subpolar front) by cyclone passage, via surface heat flux.

Procedures for making the composite maps were as follows. Of particular interest is the relatively short-term (several days) fluctuation caused by extratropical cyclones. Therefore, seasonal trends in each winter were removed using a quadratic polynomial, based on the least squares method. Thereafter, the sum of latent and sensible fluxes was averaged over the Sea of Japan (box in Figure 2a). To detect extreme flux events during the winters of 2003–2011, we chose periods when the sum of turbulent fluxes in the box was lower than -336 W m^{-2} (downward is positive, Figure 2b), corresponding to the eightieth percentile of our data set. The same threshold (eightieth) was adopted in previous studies [e.g., *Shaman et al*., 2010; *Ma et al*., 2015]. Each event was indicated by the "peak day" when the upward heat flux averaged over the box in Figure 2a met the aforementioned criterion. This should also be the local minima in the time series (solid dots in Figure 2b). Even if the events occurred consecutively, they would be recognized as a single event when they produced local minima in the daily time series. Subsequently, for all the detected events, we constructed maps of atmospheric and oceanic properties (e.g., SST) averaged daily on "peak days," and days before and after peak days.

To investigate subpolar front locations and strengths, the gradient magnitude (G) is given by:

$$G=\sqrt{\left(\frac{\partial T}{\partial x}\right)^2+\left(\frac{\partial T}{\partial y}\right)^2}, \quad (1)$$

where T represents the water temperature, and x and y indicate eastward and northward positions, respectively.

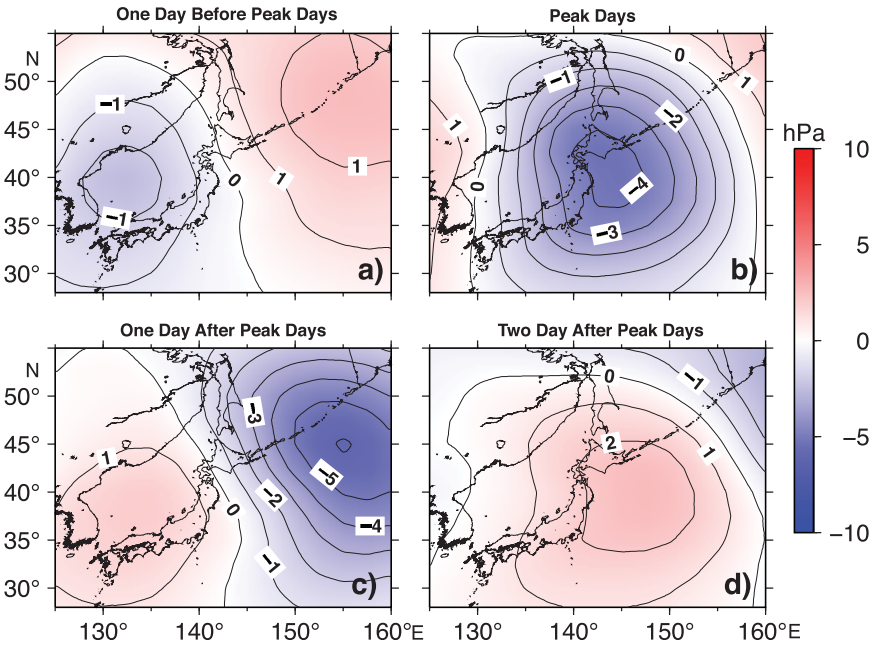

Figure 3. Composite maps of 1–8 day band-pass filtered SLP on (a) 1 day before peak days, (b) peak days, (c) 1 day after, and (d) 2 days after peak days. Contour interval is 1 hPa.

2.3. Mixed-Layer Model Analyses

The surface mixed-layer model (so-called "slab model") is likely the simplest tool to uncover the temperature modulation in the upper ocean. In the present application, we constructed such a model, in which the mixed-layer depth is defined by that at which seawater density (σ) increases by a certain value $\Delta\sigma$ from the reference depth. The values for both σ and $\Delta\sigma$ were from DREAMS data. The reference depth was set to 10 m, because the mixed layer in the Sea of Japan is always deeper than that depth during winter [*Lim et al.*, 2012]. Horizontal resolution of this model is $1/12^\circ \times 1/15^\circ$ following the DREAMS data set.

In the mixed-layer model, the time derivative of mixed-layer temperature is expressed by the sum of heat flux, horizontal heat advection, and entrainment terms. We omitted horizontal eddy diffusion because its contribution is negligibly small in determining frontal structure in the Sea of Japan [*Zhao et al.*, 2014]. Thus, the equation is

$$\frac{\partial T'_{ML}}{\partial t} = \frac{(Q_{net} - Q(-h))'}{c_p \rho h} - \mathbf{U'_{ML}} \cdot \nabla T_{ML} - \frac{w' \Delta T}{h}, \tag{2}$$

where T and $\mathbf{U}$ represent temperature and current velocities, respectively, and subscript "ML" refers to the vertically averaged value in the mixed layer. Values with prime symbols represent anomalies from the seasonal trends unrelated to the passage of cyclones, e.g., $T' = T - \bar{T}$, where the overbar represents the seasonal trend (see Appendix A for details of nonlinear anomalous term). Q_{net} denotes net heat fluxes given by OAFlux, h the mixed-layer depth, c_p the specific heat of seawater (3986 J kg^{-1} K^{-1}), and ρ seawater density (constant in the computations at 1025 kg m^{-3}). The penetrative radiative flux at the base of the mixed layer, $Q(-h)$, is given by

$$Q(-h) = Q(0)[R\exp(-h/\gamma_1) + (1-R)\exp(-h/\gamma_2)], \tag{3}$$

where $Q(0)$ is shortwave radiation at the sea surface (OAFlux). R, γ_1, and γ_2 are 0.58, 0.35, and 23, respectively, which correspond to type I water [*Paulson and Simpson*, 1977].

Entrainment speed anomaly, w', is defined as

$$w' = \left(\frac{\partial h}{\partial t}\right)' + \mathbf{u}'_{-h} \cdot \nabla h + w'_{-h}, \tag{4}$$

where $\mathbf{u}'_{-h}$ is the horizontal velocity anomaly at the base of the mixed layer. The entrainment speed was set to 0 for $w' < 0$ (upward is positive). ΔT is the temperature difference between the mixed layer and layer

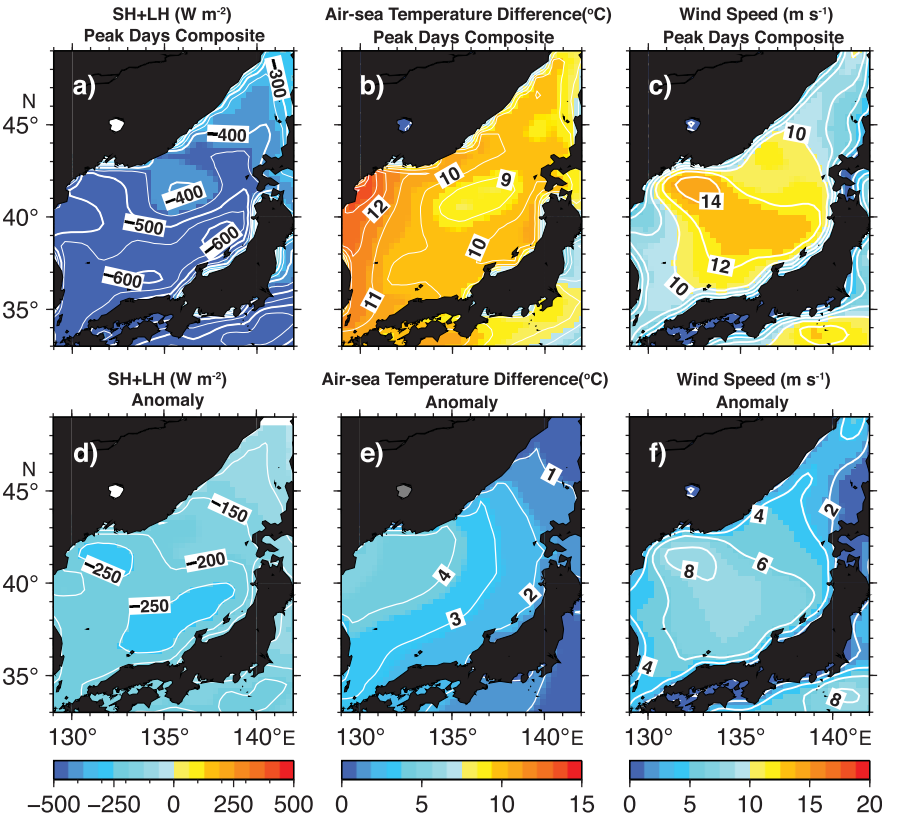

Figure 4. Composite maps of (a) turbulent fluxes (W m^{-2}), (b) air-sea temperature difference (°C), and (c) wind speed (m s^{-1}) on peak days. Lower plots also show (d) turbulent heat fluxes, (e) air-sea temperature difference, and (f) wind magnitude, but for anomalies relative to the long-term average in winter. Contour intervals of Figures 4a and 4d, 4b and 4e, and 4c and 4f are 50 W m^{-2}, 1°C, and 2 m s^{-1}, respectively.

just below (from DREAMS data). Here w'_{-h} is the anomaly of Ekman pumping velocity, computed using wind stress curl as

$$w'_{-h} = curl_z\left(\frac{\tau'}{\rho f}\right), \tag{5}$$

where τ is the wind stress vector derived from the bulk formula, $\tau = \rho_{air} C_D |\mathbf{U_{10}}| \mathbf{U_{10}}$, and $\mathbf{U_{10}}$ is the 10 m wind vector from QuikSCAT and ASCAT. Air density ρ_{air} is 1.2 kg m^{-3}, and C_D is the drag coefficient calculated following *Large and Pond* [1981].

After calculating the above heat budget equation, temporal variation of mixed-layer temperature ($\Delta T'_{ML}$) can be easily obtained as follows.

$$\begin{aligned}\Delta T'_{ML} &= \left(\frac{(Q_{net} - Q(-h))'}{c_p \rho h}\right)\Delta t + (-\mathbf{U'_{ML}} \cdot \nabla T_{ML})\Delta t + \left(-\frac{w'\Delta T}{h}\right)\Delta t, \\ &= \Delta T'_{ML_Q} + \Delta T'_{ML_A} + \Delta T'_{ML_E}\end{aligned} \tag{6}$$

where 24 h was chosen for Δt so that the excursion of anomalous currents ($<O(10)$ cm s^{-1}) was shorter than the grid spacing (1/12° and 1/15° for longitude and latitude, respectively) within the time increment. The boundary condition for T_{ML} was from DREAMS data at all straits connected to outside seas.

The computation procedure was as follows. First, T_{ML} (and h and ΔT) on the right-hand side of equation (6) was from DREAMS data on the day prior to peak days, peak days, and 1 day after peak days. Hence, $\Delta T'_{ML}$s on the peak days, 1 day after peak days, and 2 days after peak days were computed separately using equation (6). The computation was done for those 3 days because, as shown later in section 3, SST variation

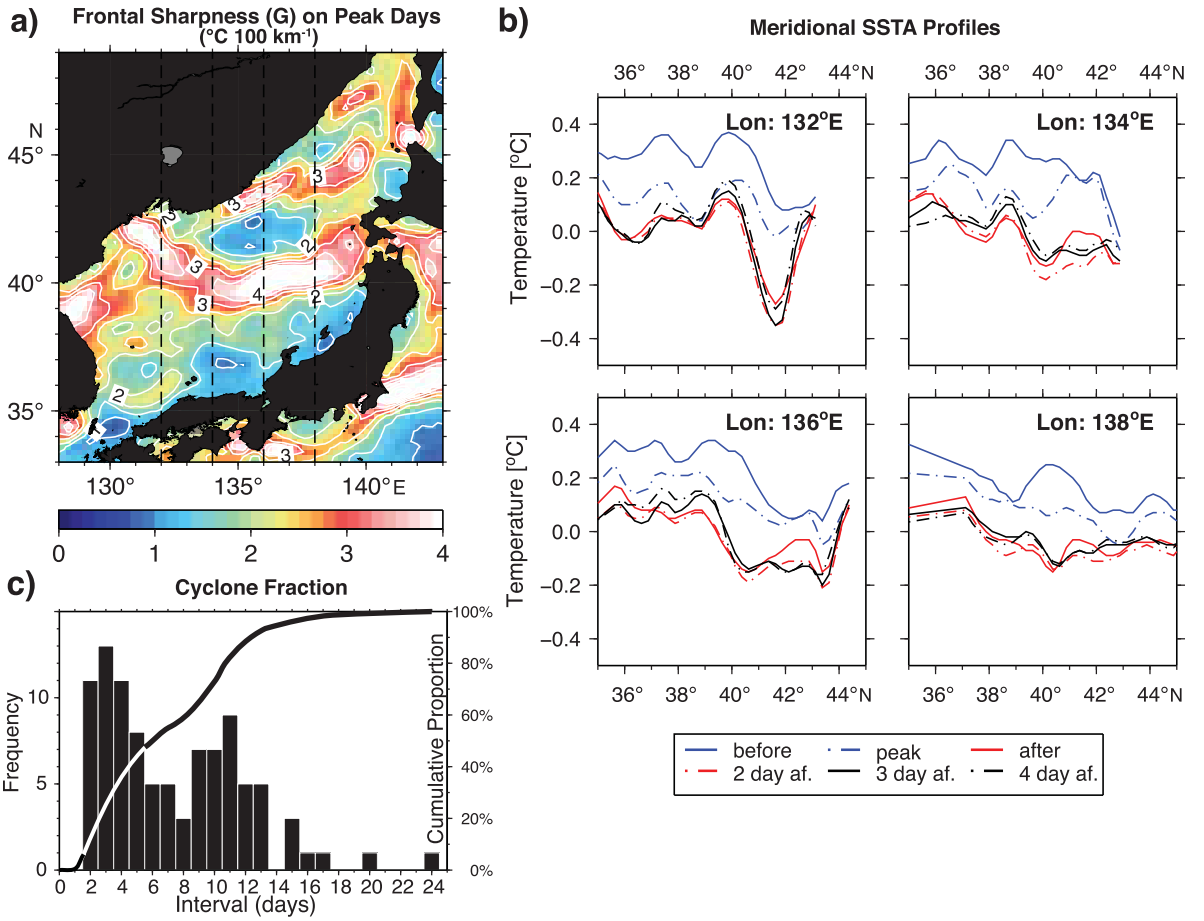

Figure 5. Relationship between temperature field and passage of extratropical cyclones. (a) The distribution of gradient magnitude (G) on peak days, by contours (every 1°C (100 km)$^{-1}$) and color shading. Dashed lines show the locations of four meridional profiles of SSTA, whose data are displayed in Figure 5b. (b) The meridional profiles are composited on six sequential days around the peak days, from 1 day before to 4 days after. (c) Frequency (digits indicate numbers) of the interval (in days) between two consecutive cyclones during 2003–2011. Their cumulative proportion is also shown by a bold solid curve.

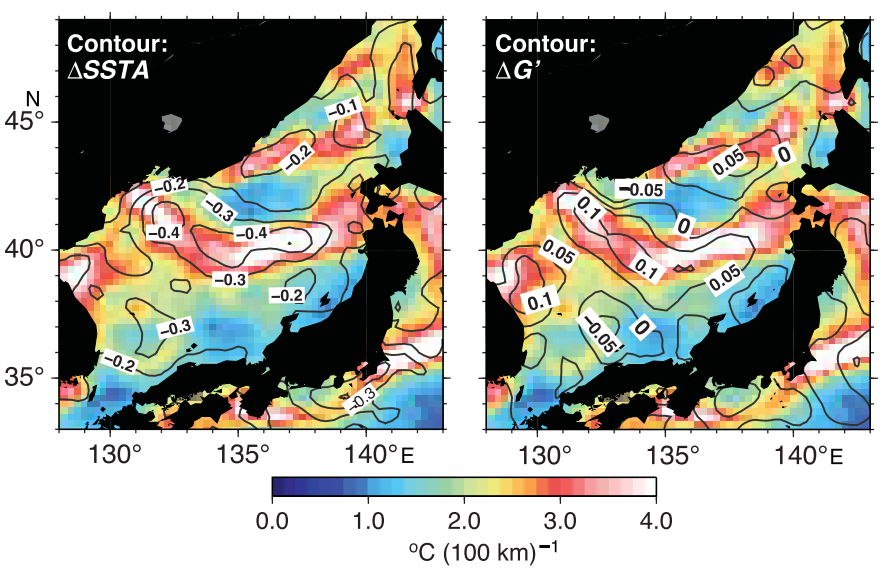

Figure 6. Composite maps of (left) temperature differences ($\Delta SSTA$) and (right) differences of gradient magnitude ($\Delta G'$) 2 days after minus 1 day before peak days, which are superimposed on frontal sharpness during peak days (color shading in both maps). Contour intervals are 0.1°C and 0.05°C (100 km)$^{-1}$, respectively.

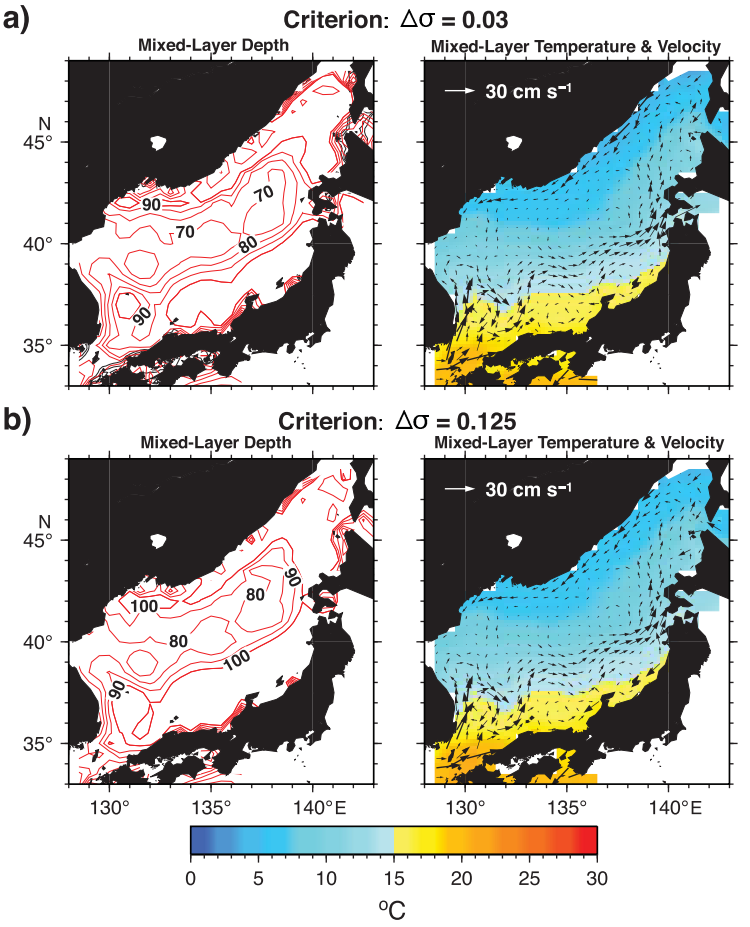

Figure 7. Mixed-layer depth (contours in left maps), mixed-layer temperature (color shading in right maps), and horizontal currents averaged over the mixed layer (vectors in right maps), provided by DREAMS data for the Sea of Japan. Figures 7a and 7b show the same properties but for different definitions of mixed-layer depth, with (a) $\Delta\sigma$=0.03 kg m^{-3} and (b) $\Delta\sigma$=0.125 kg m^{-3}.

terminated within 3 days with the passage of extratropical cyclones and surface cooling. These three time computations were conducted around all peak days over the study period; see solid dots in Figure 2b for the case of 2004–2005. Temperature increments were all summed over those computations (hence, we obtained $\Delta T'_{ML}$ 2 days after minus 1 day before peak days) and averaged over the study period.

Thereafter, we decomposed the temporal variation of gradient magnitude ($\Delta G'_{ML}$) in the mixed-layer model into contributions of heat flux ($\Delta G'_{ML_Q}$), horizontal heat advection ($\Delta G'_{ML_A}$), and entrainment ($\Delta G'_{ML_E}$), under the assumption of a linear relationship [e.g., *Kazmin and Rienecker*, 1996; *Zhao et al.*, 2014], as

$$\Delta G'_{ML} = \Delta G'_{ML_Q} + \Delta G'_{ML_A} + \Delta G'_{ML_E}. \quad (7)$$

The above three components of $\Delta G'_{ML}$ were computed separately using the corresponding three components of $\Delta T'_{ML}$ (right-hand side of equation (6)) over the 3 days). For instance, G'_{ML_Q} on the peak days was computed by substituting the "pseudo" temperature

$$T_{pseudo} = T_{ML} + \Delta T'_{ML_Q}, \quad (8)$$

into equation (1), where T_{ML} was the temperature field 1 day prior to peak days in this case. In addition to the peak days, G'_{ML_Q} was computed in the same manner for 1 day before, 1 day after, and 2 days after peak days. Then, 3 time increments of G'_{ML_Q} (i.e., $\Delta G'_{ML_Q}$) were computed using the above four G'_{ML_Q} estimates. Last, these three $\Delta G'_{ML_Q}$ estimates were summed (as $\Delta T'_{ML_Q}$) to quantify the contribution of heat flux to frontal sharpness. Likewise, the contributions of horizontal heat advection ($\Delta G'_{ML_A}$) and entrainment ($\Delta G'_{ML_E}$) to that sharpness were computed.

3. Results

Using our threshold, 104 peak days were chosen for periods of strong surface cooling during the winters of 2003–2011. As an example, a time series during winter 2004–2005 is shown in Figure 2b, in which solid dots represent the peak days. During these strong flux events, it is likely that there were extratropical cyclones developing near the Sea of Japan, since they have a typical time scale of the extratropical cyclone activity in East Asia [e.g., *Nakamura*, 1992; *Nakamura et al.*, 2002; *Isobe and Beardsley*, 2007]. However, as mentioned by *Dorman et al.* [2004], there might be some events that are not associated with cyclones. For this reason,

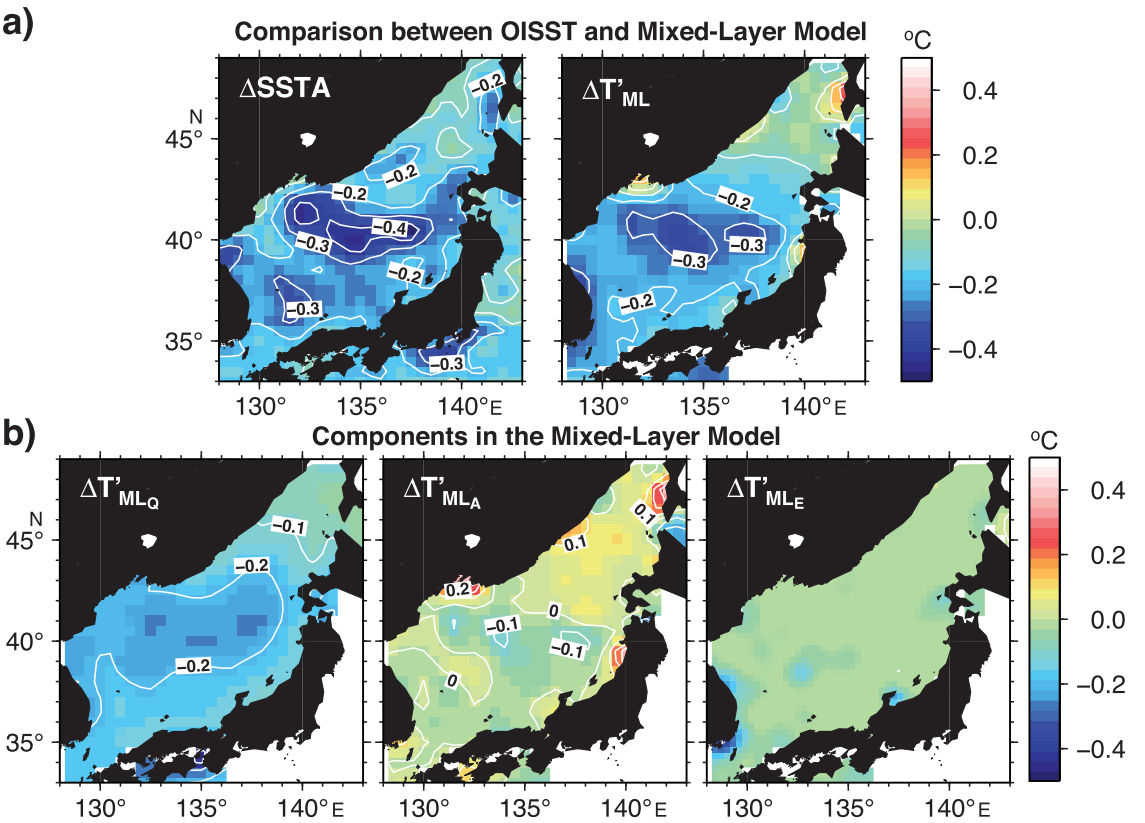

Figure 8. Temperature differences estimated as 2 days after minus 1 day before peak days (color shading and contours). (a) Temperature difference derived (left) from OISST data ($\Delta SSTA$) and (right) from mixed-layer model of present study. (b) Contributions of (left) heat flux ($\Delta T'_{ML_Q}$), (middle) horizontal heat advection ($\Delta T'_{ML_A}$), and (right) entrainment ($\Delta T'_{ML_E}$) to SST reduction in Figure 8a. For ease of comparison with OISST data, results were smoothed onto coarse grids ($1/4^\circ \times 1/4^\circ$) as used by OISST data. Contour intervals of all maps are 0.1°C.

we visually checked all SLP maps for removal of the noncyclone days, resulting in 102 days for subsequent analyses.

Composite maps of 1–8 day band-pass filtered SLP around peak days clearly demonstrate strong cooling when extratropical cyclones developed around the Sea of Japan (Figure 3). A low-pressure system west of that sea strengthened rapidly from 1 day before peak days (Figure 3a) to peak days (Figure 3b). Strong northerly winds (and thus sea surface cooling) are indicated by tightly packed SLP contours over the sea on the peak days. Only 1 day after peak days, the low-pressure system center moved to the south of the Kamchatka Peninsula (at the northeast corner of the map), and the central pressure deepened from −1 to −6 hPa (Figures 3a–3c). The system moved further northeast and left the figure domain on 2 days after peak days (Figure 3d). As the low center moved northeastward, the filtered SLP over the Sea of Japan increased (from Figures 3b–3d), suggesting that both northerly winds and upward heat flux were subdued. It is therefore obvious that these sequential 4 days categorized by heat flux effectively represented a time series of developing extratropical cyclones near the Sea of Japan, as the examples show in Figure 1.

The composite maps of turbulent fluxes, air-sea temperature differences, and wind speeds clearly demonstrate how extratropical cyclones modified the Sea of Japan on the peak days (Figure 4). The map of wind speed clearly shows a strong cold-air outbreak over the sea, across which the extratropical cyclones passed. Hence, strong surface cooling ($<$–400 W m^{-2}) covered the entire sea (Figure 4a), although upward heat flux in the south was greater than in the north. This inhomogeneity of heat flux is likely attributable to the SST distribution across the Sea of Japan, where the Tsushima Warm Current empties into its southern portion. Nevertheless, the anomaly of turbulent fluxes from the winter average reveals cooling associated with the cold-air outbreak under strong northwesterly wind (see contours of −250 W m^{-2} in Figure 4d and wind speed in Figure 4c). During the cold-air outbreak, the air-sea temperature difference reached 12°C (Figure 4b), 4°C greater than the average over the Sea of Japan during winter [*Choi and Zhang*, 2005]. Although the cold air is heated upon moving southeastward over the relatively warm ocean, that air affected the entire

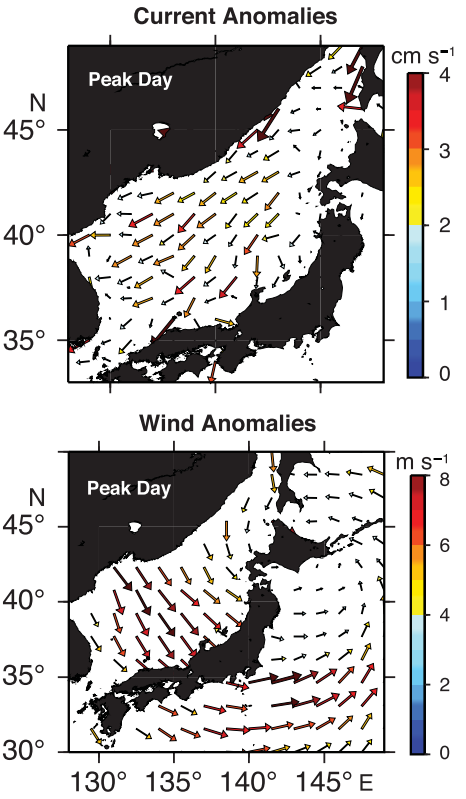

Figure 9. (top) Current and (bottom) wind anomalies on peak days. To avoid overcrowding, current vectors are plotted every sixth grid. Speeds of current and wind are shown by vector colors and length.

Sea of Japan because the anomaly of the difference remained 2°C even when the cold-air mass reached the Japanese archipelago. In addition to the air-sea temperature difference, the cold air effect across the entire sea is evident in the wind field. A jet-like northwesterly wind (greater than 14 m s^{-1}) was evident near Vladivostok because of an orographic gap (Figure 4c) [*Kawamura and Wu*, 1998], from which a wind speed of 6 m s^{-1} higher than the winter average extends southeastward (Figure 4f). The combination of the anomalous air-sea temperature difference and wind speed produced the strong cooling that prevailed across the Sea of Japan during the cold-air outbreak associated with extratropical cyclone passage.

After removal of the seasonal trends, temporal variations of meridional SST anomaly (SSTA) profiles across the subpolar front (see lines on the map of G (equation (1)) in Figure 5a) show that the time scale required for SST reduction over the Sea of Japan is around 3 days during cyclone passage (Figure 5b). First, the temperature decreased about 0.1–0.2°C on the peak days, decreasing by another 0.1–0.2°C during subsequent peak days. Thereafter, SSTA declined slightly from 1 day (red curve in Figure 5b) to 2 days (dash-dot curve) after the peak days. The reduced temperature remained cool even on 4 days after the peak days. Moreover, the frequency of winter cyclones (i.e., intervals between peak days; Figure 5c) shows that nearly half (45%; see right ordinate in Figure 5c) arrived within 4 days after the prior cyclone passage. These short intervals imply that, as speculated in the introduction, extratropical cyclones over the Sea of Japan may be affected by prior cyclones because of altered SST and/or frontal sharpness [*Graff and LaCasce*, 2012]. However, the present study did not treat this potential two-way coupling, because the objective was to elucidate a "preconditioning" revealed by temperature, i.e., subpolar front modulation by the passage of earlier cyclones.

Of particular interest is how much SST was reduced by a single cyclone (i.e., cooling) during the typical time scale of passage (we selected "3 days" in the present study because of the tallest bar in Figure 5c). We thereby estimated the reduction by taking the difference between SSTAs 1 day before and 2 days after peak days. As shown in Figure 6 (left), SST across the entire Sea of Japan cooled by $>$0.2°C on average after the passage of a single cyclone. It is interesting that this SST reduction was not homogenous across the sea but was locally great along the subpolar front, with a maximum of $>$0.4°C. This cooling pattern substantially deviates from the patterns of turbulent heat flux (Figure 4) which shows that it is the ocean process (likely within the mixed layer) that strongly contributes to the cooling pattern and the change in front, not the heat flux itself.

This temperature reduction contributed more than half (51.4%) of the total cooling (without detrending) during these 3 days, and it increased to $>$60% around the subpolar front (not shown). Further, the sharpness of the subpolar front intensified (i.e., frontogenesis) by $\sim$0.1°C (100 km)$^{-1}$ (3–4% of total frontal sharpness) after the passage of a single developing cyclone (Figure 6, right). The SST reduction and frontogenesis were both relatively small but statistically significant, as suggested by a *t* test with 95% confidence level. Moreover, the intensification of frontal sharpness covered not only over the subpolar front but also the southern regions (see the 0°C (100 km)$^{-1}$ contour in Figure 6, right). This suggests that the subpolar front was likely to shift southward, enhancing its sharpness with the passage of a single extratropical cyclone. Although further examinations will be required, it is speculated that the synoptic location of the subpolar front may be determined by the tug of war between the cyclones trying to push the front southward (and

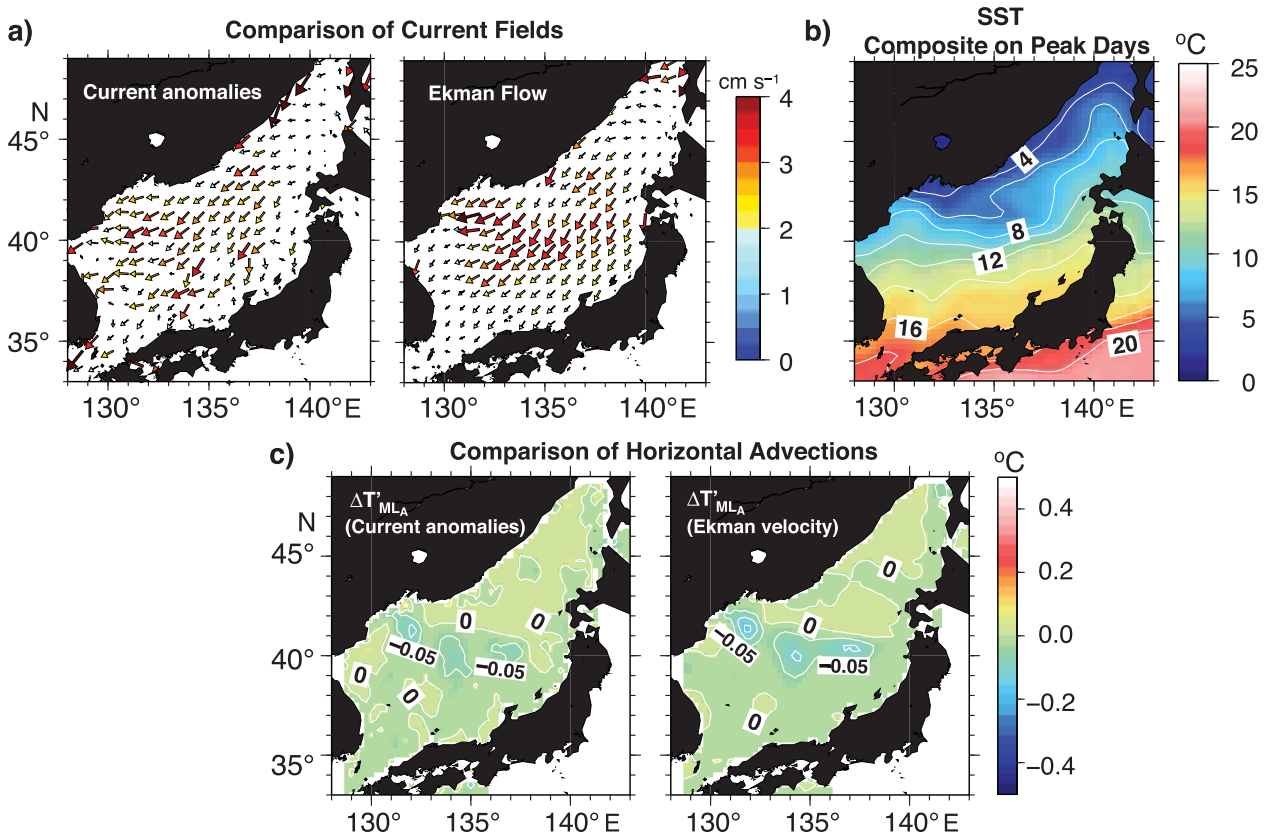

Figure 10. Comparison between current anomalies and Ekman flow. (a) (left) Current anomalies obtained from DREAMS (same as Figure 9 but at higher resolution) and (right) Ekman flow calculated from either QuikSCAT or ASCAT. Wind speed is represented by vector colors and length. (b) SST map composited for the peak days using OISST data. (c) Temperature reduction estimated using the values in Figures 10a and 10b for 24 h on peak days. Contour intervals are 2°C and 0.05°C in Figures 10b and 10c, respectively.

thus intensifying it) and the Tsushima Warm Current or the insolation that acts to restore the front location to where it is supposed to be.

4. Discussion

4.1. SST Reduction

Before addressing the cause(s) of the aforementioned SST reduction using the mixed-layer model, we must ensure that our conclusions are robust, and will not be largely influenced by the definition of the mixed-layer depth. Figure 7 shows that mixed-layer depth (left) and mixed-layer averaged temperature and current fields (right) were nearly independent of the choice of $\Delta\sigma$. Thus, for simplicity, we only show results of the case with $\Delta\sigma = 0.03$ kg m^{-3} in the following sections.

The result of the mixed-layer model was compared with the aforementioned SST reductions based on OISST data during the cold-air outbreaks associated with extratropical cyclones (Figure 8). As suggested by the temporal variations of meridional profiles (Figure 5b), we show the temperature increment over 3 days, i.e., 2 days after minus 1 day before peak days, using equation (6). For ease of comparison, model results with DREAMS resolution were smoothed to the same grid size as the OISST data set (1/4°). Figure 8a shows that the mixed-layer model did a reasonable job of reproducing a "local" cooling along the frontal zones at 40°N. Model results show that temperature reduction was less than the $\Delta SSTA$ by 0.1°C, probably because of vertical integration over the mixed layer, rather than the sea surface observation from satellites.

The contributions of each component (Figure 8b) show that the surface cooling along the subpolar front results mainly from the heat flux (greater than −0.2°C). SST reduction derived from the heat flux ($\Delta T'_{ML_Q}$) was widespread over the area from 38°N to 42°N, with the maximum at the area center. The horizontal pattern of turbulent flux anomalies (Figure 4d) caused by the cold-air outbreak is unlikely to explain the

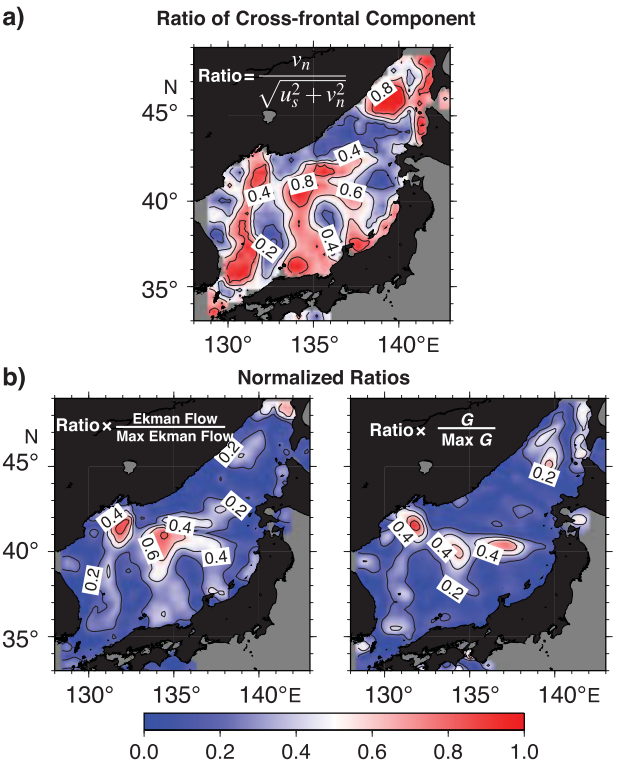

Figure 11. (a) Ratio of cross-frontal component (v_n) to total Ekman flow ($\sqrt{v_n^2+u_s^2}$) and (b) ratios normalized by the maximum Ekman flow (left: (a) $\times(\sqrt{v_n^2+u_s^2}/(\sqrt{v_n^2+u_s^2})_{Max})$) and maximum frontal sharpness (right: (a) $\times(G/(G)_{Max})$). Subscript "Max" denotes the maximum value in the study area. Contour interval is 0.2.

localization along the subpolar front. Thus, $\Delta T'_{ML_Q}$ should be controlled by mixed-layer depth (Figure 7, left), such that a relatively shallower (deeper) mixed layer causes a larger (smaller) SST reduction because of a difference in heat capacity. By comparing the mixed-layer depth and current map (Figure 7), we can see that the shallow mixed layer in the central Sea of Japan is associated with a cyclonic ocean circulation in a geostrophic sense, especially over the northern region.

Nonetheless, heat flux is the dominant contributor to the localized cooling along the subpolar front. Horizontal heat advection ($\Delta T'_{ML_A}$) provides a nonnegligible fraction (-0.1°C) of the temperature reduction along the front and is further discussed in the next section. Unlike the other two components, the entrainment ($\Delta T'_{ML_E}$) only generates substantial SST cooling (more than -0.2°C) far from the front, and its contribution is negligibly small over most of the Sea of Japan. The small entrainment contribution may result partly from the deeper mixed layer in our analyses (~70 m; see the frontal region in Figure 7) than that estimated in other studies such as *Lim et al.* [2012] (30–50 m; see their Figure 9) because of different data sets and criteria. Nonetheless, our analyses are still acceptable because observed temperature differences are consistent with the modeled ones (Figure 8a).

4.2. Localized Cooling

Aside from the turbulent heat fluxes associated with mixed-layer depth, further examination is required to uncover the cause of localized cooling along the subpolar front from horizontal heat advection. The current anomalies relative to winter trend provided in the DREAMS data (Figure 9, top) show that during the passage of extratropical cyclones, there was a nearly uniform southwestward surface current over the Sea of Japan on the peak days. These detrended current anomalies occupy the entire sea, so we must find a driving force with spatial scale larger than the sea and temporal scale shorter than the winter season. Northwesterly wind anomalies associated with synoptic-scale extratropical cyclones (Figure 3b and Figure 9, bottom) are consistent with the southwestward current anomalies in the sense of the Ekman flow (defined by $\tau/\rho fh$ in this study). Therefore, it is believed that this strong northwesterly wind, triggered by cyclone passage, engenders southwestward (cross-frontal) Ekman flow, which transports the cold water mass that ultimately causes the local SST reduction along the front.

To confirm the above scenario, we computed Ekman flow using the wind anomalies (Figure 10a) to compare with the current anomalies from the DREAMS data set. Current anomalies included small-scale features, probably because of the superposition of mesoscale (on the order of ~ several hundreds of kilometers) eddies. Thus, the anomalous currents are slightly weaker than the Ekman flow. Nonetheless, both represent the same large-scale southwestward flows. In addition, strong current anomalies were found in the central Sea of Japan. To examine whether these current fields could cause the localized cooling along the subpolar front, we calculated horizontal heat advection on the peak days using these two current fields in conjunction with the composite SST field from OISST (Figure 10b). Figure 10c shows that the temperature

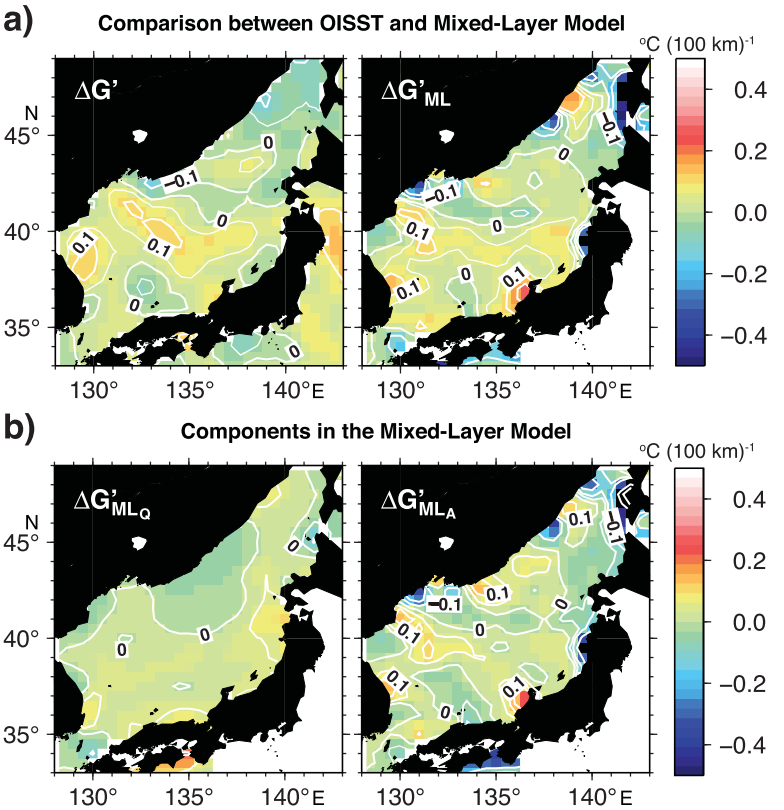

Figure 12. Comparison of differences of gradient magnitude ($\Delta G'$).(a) Estimated $\Delta G'$ for 2 days after minus 1 day before peak days based on OISST data (left; same as the right figure in Figure 6). Right figure is the same as the left but for mixed-layer model. (b) Contributions of (left) heat flux ($\Delta G'_{ML_Q}$) and (right) horizontal heat advection ($\Delta G'_{ML_A}$) to $\Delta G'_{ML}$ computed by the mixed-layer model. As in Figure 8, results were smoothed onto coarse grids ($1/4° \times 1/4°$). Contour intervals of all figures are 0.05°C (100 km)$^{-1}$.

reduction that results from horizontal heat advection by the current anomalies is reasonably consistent with that by Ekman flow.

For more quantitative assessment of this basin-wide southwestward Ekman flow, we separated it into cross-frontal (v_n, normal to the isotherms) and along-frontal (u_s, along the isotherms) components, using curvilinear natural coordinates as follows.

$$\begin{aligned} v_n &= -sin\varphi\, u + cos\varphi\, v, \\ u_s &= cos\varphi\, u + sin\varphi\, v, \end{aligned} \tag{9}$$

where u and v are the Ekman flows in the zonal and meridional Cartesian directions, respectively, and φ represents the counterclockwise isotherm direction relative to the x axis.

Figure 11a shows that this southwestward Ekman flow was approximately parallel to isotherms north of the subpolar front (42°N–45°N), while the cross-frontal components dominated in other areas, especially near the front (over 60% of total flow). To dramatize the importance of the cross-frontal component around the subpolar front, we normalized this component in two ways. After the normalization by current speed, vigorous cross-frontal Ekman flow was revealed north of 40°N (Figure 11b, left). Intensification of the cross-frontal Ekman flow at the front is similar to the observed results in *Thomas and Lee* [2005]. However, their intensification was within a narrow band (<10 km; see their Figure 11), 1 order of magnitude smaller than our area (Figure 11b). In our study, such a pattern was mainly caused by the jet-like wind field that formed by the topography along the Russian coast (see wind speed in Figure 4c and vectors in Figure 9, bottom) and partially by the shallow mixed-layer depth (inversely proportional to Ekman flow) around the front (Figure 7, left). After the normalization by frontal sharpness (G, in equation (1)), heat advection locally reduced the temperature via this cross-frontal Ekman flow at the frontal region (clearly revealed by Figure 11b, right).

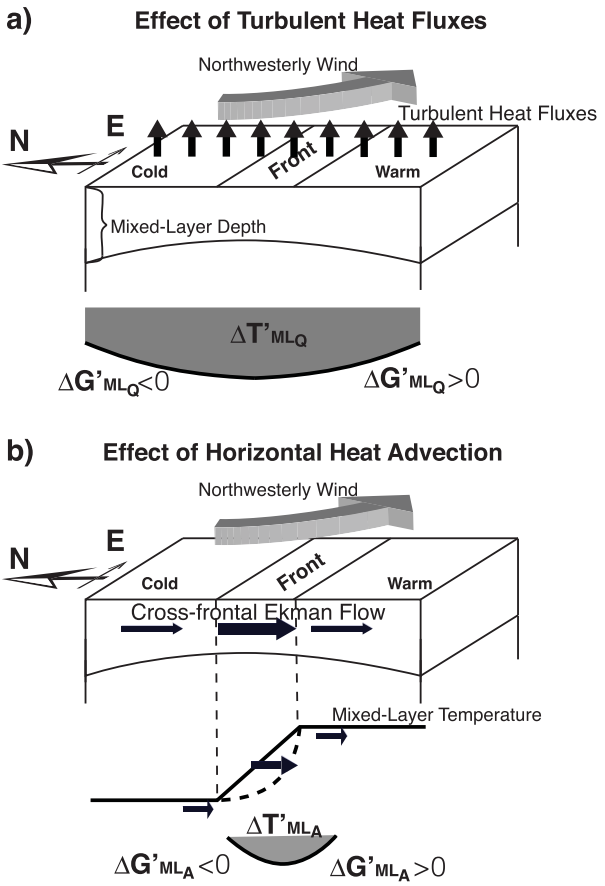

Figure 13. Schematic views of the (a) effects of turbulent heat fluxes and (b) horizontal heat advection during passage of extratropical cyclones. Thick gray arrow represents strong northwesterly wind associated with the cyclones. In both figures, gray shading in lower portions shows temperature reduction caused by turbulent heat fluxes ($\Delta T'_{ML_Q}$) and horizontal heat advection ($\Delta T'_{ML_A}$), and slopes of solid curves represent changes of frontal sharpness ($\Delta G'_{ML_Q}$ and $\Delta G'_{ML_A}$).

It is possible that a frontogenetic process associated with ageostrophic secondary circulations and Ekman pumping/suctions occurs locally along the frontal interface, as shown by theoretical and nonhydrostatic numerical models in *Thomas and Lee* [2005] and *Yoshikawa et al*. [2012]. However, their studies are not applicable to the process revealed by the present analysis. Much finer temporal (subinertial time scale) and spatial (<10 km) scales are both required for reproducing such processes and, as such, could not be captured by our mixed-layer model and data sets. Nonetheless, the aforementioned studies suggest that the sharpness of the subpolar front would be enhanced more than we expected if the fine-scale processes are incorporated in a numerical model approach.

4.3. Contribution to Frontogenesis

Figure 6 (right) shows that the gradient magnitude increased by ~0.1°C (100 km)$^{-1}$ along the subpolar front, because of the passage of a single extratropical cyclone. Using equation (7), we calculated the contributions of heat flux ($\Delta G'_{ML_Q}$) and horizontal heat advection ($\Delta G'_{ML_A}$) to the enhancement of frontal sharpness (note that the entrainment is excluded here, because its effect is negligibly small). The sum of these two components is shown in Figure 12a, and each contribution is depicted in Figure 12b. The modeled results reproduced frontogenesis well, in both magnitude and locations. Also shown by Figure 12a is that the linear assumption of equation (7) is likely to be justified because the sum of the two components is nearly identical to $\Delta G'$. Looking at each contribution (Figure 12b), one sees that heat flux has a secondary effect on the frontogenesis, although that flux accounts for about two thirds of SST reduction (Figure 8b). This is because the heat flux has a spatial scale much larger than the width of the subpolar front. However, even with one third of the contribution to SST reduction (Figure 8b), the horizontal heat advection can be regarded as the primary enhancement of frontal sharpness (see similarity to Figure 8a), because of the localized cooling along the front.

5. Conclusion

The mechanisms of SST reduction and frontogenesis in the winter Sea of Japan are summarized below (Figure 13). Developing extratropical cyclones induce strong cold-air outbreaks, accompanied by strong northwesterly winds transporting a cold-air mass over the entire Sea of Japan. During the cooling event, SST in the central sea is reduced remarkably because of the shallowness of the mixed layer. Upward heat flux intensifies the sharpness of the subpolar front (Figure 13a), in spite of a contribution much smaller than that of horizontal heat advection. Meanwhile, the strong northwesterly wind generates a strong cross-frontal Ekman flow, transporting the cold water across the isotherms. This further reduces the temperature locally along the subpolar front and intensifies the front, representing the primary contributor (Figure 13b).

These results are apparently different from studies of wind-driven frontogenesis associated with fine-scale dynamics.

Overall, our analyses show that the subpolar front in the Sea of Japan intensifies after passage of a developing extratropical cyclone. Therefore, the suggestion is the formation of a two-way coupling process between the SST (hence the sharp subpolar front) and the extratropical cyclones. Many studies have demonstrated that enhanced frontal sharpness intensifies cyclones [e.g., *Yamamoto and Hirose*, 2007] and/or alters their trajectories via an anchoring effect [e.g., *Ogawa et al*., 2012]. There remains a question as to how such hydrographical changes in the Sea of Japan affect subsequent extratropical cyclones. This should be addressed in our next study.

It should be noted that the cyclone-induced SST reduction may also be included in the seasonal trend, because the temperature reduction of a single cyclone is not always recovered completely after cyclone passage. It is, however, difficult to separate this contribution from the seasonal trend using the present data analyses. The time scale of SST recovery (by horizontal heat advection, eddy-induced heat transport, and subgrid-scale horizontal diffusion) must be a critical factor, and the aforementioned two-way coupling processes complicate the problem. SST recovery processes are a major scientific issue in the physical oceanography. For instance, although *Mei and Pasquero* [2013] suggested that the SST recovery time varies considerably by case, in general, recovery from SST cooling by tropical cyclones occurs on an intra-seasonal time scale (around 5–30 days) [*Dare and Mcbirde*, 2011]. We may expect a similar time scale of SST recovery, even at midlatitudes. A numerical model approach incorporating a two-way coupling process is likely required to answer the above questions, so this will also be the next step in the near future.

Appendix A: Derivation of Nonlinear Anomalous Term in Equation (2)

For example, an anomalous temperature (T') is derived as

$$T' = T - \bar{T}, \tag{A1}$$

where the overbar represents the seasonal trend. Substituting anomalies and seasonal trend into the nonlinear term (horizontal advection, $\mathbf{U} \cdot \nabla T$) yields

$$(\mathbf{U}' + \overline{\mathbf{U}}) \cdot \nabla (T' + \bar{T}) = \overline{\mathbf{U}} \cdot \nabla \bar{T} + \overline{\mathbf{U}} \cdot \nabla T' + \mathbf{U}' \cdot \nabla T. \tag{A2}$$

The first term in the right-hand side is the seasonal trend of the advection term which should be removed. During our data processing, we also found that the second term is 1 order smaller (O(0.01°C), not shown) than the third term (O(0.1°C)). Therefore, the nonlinear anomalous advection term can be defined by $\mathbf{U}' \cdot \nabla T$ as described in equation (2).

Acknowledgments
The authors thank the gridded data set providers, including the WHOI OAFlux project, NOAA/OAR/ESRL PSD (http://www.esrl.noaa.gov/psd), and Research Institute for Applied Mechanics (RIAM) of Kyushu University. QuikSCAT and C-2013 ASCAT data are produced by Remote Sensing Systems and sponsored by the NASA Ocean Vector Winds Science Team. We also thank two anonymous reviewers for their valuable comments and the Editor of JGR-Oceans for his effective work. This work was partially supported by the Ministry of Education, Culture, Sports, Science and Technology of Japan, KAKENHI (#22106002).

References

Belkin, I., and P. Cornillon (2003), SST fronts of the Pacific coastal and marginal seas, *Pac. Oceanogr.*, *1*(2), 90–113.

Chen, S.-J., Y.-H. Kuo, P.-Z. Zhang, and Q.-F. Bai (1991), Synoptic climatology of cyclogenesis over East Asia, 1958-1987, *Mon. Weather Rev.*, *119*(6), 1407–1418.

Chen, S.-J., Y.-H. Kuo, P.-Z. Zhang, and Q.-F. Bai (1992), Climatology of explosive cyclones off the East Asian coast, *Mon. Weather Rev.*, *120*(12), 3029–3035.

Choi, H., and Y. Zhang (2005), Monthly variation of sea-air temperature differences in the Korean coast, *J. Oceanogr.*, *61*(2), 359–367, doi:10.1007/s10872-005-0046-y.

Dare, R. A., and J. L. Mcbride (2011), Sea surface temperature response to tropical cyclones, *Mon. Weather Rev.*, *139*(12), 3798–3808, doi:10.1175/MWR-D-10-05019.1.

Dorman, C. E., R. C. Beardsley, N. Dashko, C. Friehe, D. Kheilf, K. Cho, R. Limeburner, and S. Varlamov (2004), Winter marine atmospheric conditions over the Sea of Japan, *J. Geophys. Res.*, *109*, C12011, doi:10.1029/2001JC001197.

Graff, L. S., and J. LaCasce (2012), Changes in the extratropical storm tracks in response to changes in SST in an AGCM, *J. Clim.*, *25*(6), 1854–1870, doi:10.1175/JCLI-D-11-00174.1.

Hirose, N., K. Nishimura, and M. Yamamoto (2009), Observational evidence of a warm ocean current preceding a winter teleconnection pattern in the Northwestern Pacific, *Geophys. Res. Lett.*, *36*, L09705, doi:10.1029/2009GL037448.

Hirose, N., K. Takayama, J.-H. Moon, T. Watanabe, and Y. Nishida (2013), Regional data assimilation system extended to the East Asian marginal seas, *Umi to Sora (Sea and Sky)*, *89*(2), 1–9.

Inatsu, M., H. Mukougawa, and S.-P. Xie (2003), Atmospheric response to zonal variations in midlatitude SST: Transient and stationary eddies and their feedback, *J. Clim.*, *16*(20), 3314–3329.

Isobe, A., and R. C. Beardsley (2007), Atmosphere and marginal-sea interaction leading to an interannual variation in cold-air outbreak activity over the Sea of Japan, *J. Clim.*, *20*(23), 5707–5714, doi:10.1175/2007JCLI1779.1.

Isobe, A., and S. Kako (2012), A role of the Yellow and East China Seas in the development of extratropical cyclones in winter, *J. Clim.*, *25*(23), 8328–8340, doi:10.1175/JCLI-D-11-00391.1.
Isoda, Y. (1994), Interannual SST variations to the north and south of the polar front in the Sea of Japan, *La Mer*, *32*, 285–293.
Iwasaki, S., A. Isobe, and S. Kako (2014), Atmosphere–ocean coupled process along coastal areas of the Yellow and East China Seas in winter, *J. Clim.*, *27*(1), 155–167, doi:10.1175/JCLI-D-13-00117.1.
Kanamitsu, M., W. Ebisuzaki, J. Woollen, S.-K. Yang, J. Hnilo, M. Fiorino, and G. Potter (2002), NCEP-DOE AMIP-II Reanalysis (R-2), *Bull. Am. Meteorol. Soc.*, *83*(11), 1631–1643, doi:10.1175/BAMS-83-11-1631.
Kawamura, H., and P. Wu (1998), Formation mechanism of Sea of Japan proper water in the flux center off Vladivostok, *J. Geophys. Res.*, *103*(C10), 21,611–21,622, doi:10.1029/98JC01948.
Kazmin, A. S., and M. M. Rienecker (1996), Variability and frontogenesis in the large-scale oceanic frontal zones, *J. Geophys. Res.*, *101*(C1), 907–921, doi:10.1029/95JC02992.
Kelly, K. A., R. J. Small, R. Samelson, B. Qiu, T. M. Joyce, Y.-O. Kwon, and M. F. Cronin (2010), Western boundary currents and frontal air-sea interaction: Gulf stream and Kuroshio Extension, *J. Clim.*, *23*(21), 5644–5667, doi:10.1175/2010JCLI3346.1.
Large, W., and S. Pond (1981), Open ocean momentum flux measurements in moderate to strong winds, *J. Phys. Oceanogr.*, *11*(3), 324–336.
Lim, S., C. J. Jang, I. S. Oh, and J. Park (2012), Climatology of the mixed layer depth in the East/Sea of Japan, *J. Mar. Syst.*, *96*, 1–14, doi:10.1016/j.jmarsys.2012.01.003.
Ma, X., P. Chang, R. Saravanan, D. Wu, X. Lin, L. Wu, and X. Wan (2015), Winter extreme flux events in the Kuroshio and Gulf Stream extension regions and relationship with modes of North Pacific and Atlantic variability *J. Clim.*, *28*(12), 4950–4970, doi:10.1175/JCLI-D-14-00642.1.
Mei, W., and C. Pasquero (2013), Spatial and temporal characterization of sea surface temperature response to tropical cyclones, *J. Clim.*, *26*(11), 3745–3765, doi:10.1175/JCLI-D-12-00125.1.
Minobe, S., A. Kuwano-Yoshida, N. Komori, S.-P. Xie, and R. J. Small (2008), Influence of the Gulf Stream on the troposphere, *Nature*, *452*(7184), 206–209, doi:10.1038/nature06690.
Nakamura, H. (1992), Midwinter suppression of baroclinic wave activity in the Pacific, *J. Atmos. Sci.*, *49*(17), 1629–1642.
Nakamura, H., T. Izumi, and T. Sampe (2002), Interannual and decadal modulations recently observed in the Pacific storm track activity and East Asian winter monsoon, *J. Clim.*, *15*(14), 1855–1874.
Nakamura, H., T. Sampe, Y. Tanimoto, and A. Shimpo (2004), Observed associations among storm tracks, jet streams and midlatitude oceanic fronts, in *Earth's Climate: The Ocean–Atmosphere Interaction, Geophys. Monogr. Ser.*, vol. 147, edited by C. Wang, S.-P. Xie, and J. A. Carton, pp. 329–345, AGU, Washington, D. C., doi:10.1029/147GM18.
Nonaka, M., H. Nakamura, B. Taguchi, N. Komori, A. Kuwano-Yoshida, and K. Takaya (2009), Air-sea heat exchanges characteristic of a prominent midlatitude oceanic front in the South Indian Ocean as simulated in a high-resolution coupled GCM, *J. Clim.*, *22*(24), 6515–6535, doi:10.1175/2009JCLI2960.1.
Ogawa, F., H. Nakamura, K. Nishii, T. Miyasaka, and A. Kuwano-Yoshida (2012), Dependence of the climatological axial latitudes of the tropospheric westerlies and storm tracks on the latitude of an extratropical oceanic front, *Geophys. Res. Lett.*, *39*, L05804, doi:10.1029/2011GL049922.
Overland, J. E., J. M. Adams, and N. A. Bond (1999), Decadal variability of the Aleutian Low and its relation to high-latitude circulation, *J. Clim.*, *12*(5), 1542–1548.
Papritz, L., S. Pfahl, H. Sodemann, and H. Wernli (2015), A climatology of cold air outbreaks and their impact on air-sea heat fluxes in the high-latitude South Pacific, *J. Clim.*, *28*(1), 342–364, doi:10.1175/JCLI-D-14-00482.1.
Paulson, C. A., and J. J. Simpson (1977), Irradiance measurements in the upper ocean, *J. Phys. Oceanogr.*, *7*(6), 952–956.
Reynolds, R. W., T. M. Smith, C. Liu, D. B. Chelton, K. S. Casey, and M. G. Schlax (2007), Daily high-resolution-blended analyses for sea surface temperature, *J. Clim.*, *20*(22), 5473–5496, doi:10.1175/2007JCLI1824.1.
Sampe, T., H. Nakamura, A. Goto, and W. Ohfuchi (2010), Significance of a midlatitude SST frontal zone in the formation of a storm track and an eddy-driven westerly jet, *J. Clim.*, *23*(7), 1793–1814, doi:10.1175/2009JCLI3163.1.
Seo, H., Y.-O. Kwon, and J.-J. Park (2014), On the effect of the East/Sea of Japan SST variability on the North Pacific atmospheric circulation in a regional climate model, *J. Geophys. Res. Atmos.*, *119*, 418–444, doi:10.1002/2013JD020523.
Shaman, J., R. M. Samelson, and E. Skyllingstad (2010), AirSea fluxes over the Gulf Stream region: Atmospheric controls and trends, *J. Clim.*, *23*(10), 2651–2670, doi:10.1175/2010JCLI3269.1.
Small, R., S. P. deSzoeke, S. Xie, L. ONeill, H. Seo, Q. Song, P. Cornillon, M. Spall, and S. Minobe (2008), Air-sea interaction over ocean fronts and eddies, *Dyn. Atmos. Oceans*, *45*(3), 274–319, doi:10.1016/j.dynatmoce.2008.01.001.
Thomas, L. N., and C. M. Lee (2005), Intensification of ocean fronts by down-front winds, *J. Phys. Oceanogr.*, *35*(6), 1086–1102, doi:10.1175/JPO2737.1.
Trenberth, K. E., W. G. Large, and J. G. Olson (1990), The mean annual cycle in global ocean wind stress, *J. Phys. Oceanogr.*, *20*(11), 1742–1760.
Yamamoto, M. (2013), Effects of a semienclosed ocean on extratropical cyclogenesis: The dynamical processes around the Sea of Japan on 23–25 January 2008, *J. Geophys. Res. Atmos.*, *118*, 10–391, doi:10.1002/jgrd.50802.
Yamamoto, M., and N. Hirose (2007), Impact of SST reanalyzed using OGCM on weather simulation: A case of a developing cyclone in the Sea of Japan area, *Geophys. Res. Lett.*, *34*, L05808, doi:10.1029/2006GL028386.
Yamamoto, M., and N. Hirose (2011), Possible modification of atmospheric circulation over the Northwestern Pacific induced by a small semi-enclosed ocean, *Geophys. Res. Lett.*, *38*, L03804, doi:10.1029/2010GL046214.
Yoshiike, S., and R. Kawamura (2009), Influence of wintertime large-scale circulation on the explosively developing cyclones over the Western North Pacific and their downstream effects, *J. Geophys. Res.*, *114*, D13110, doi:10.1029/2009JD011820.
Yoshikawa, Y., C. M. Lee, and L. N. Thomas (2012), The subpolar front of the Japan/East Sea. Part III: Competing roles of frontal dynamics and atmospheric forcing in driving ageostrophic vertical circulation and subduction, *J. Phys. Oceanogr.*, *42*(6), 991–1011, doi:10.1175/JPO-D-11-0154.1.
Zhao, N., A. Manda, and Z. Han (2014), Frontogenesis and frontolysis of the subpolar front in the surface mixed layer of the Sea of Japan, *J. Geophys. Res. Oceans*, *119*, 1498–1509, doi:10.1002/2013JC009419.
Zolina, O., and S. K. Gulev (2003), Synoptic variability of ocean-atmosphere turbulent fluxes associated with atmospheric cyclones, *J. Clim.*, *16*(16), 2717–2734.